

- 1533 (1995); S. Dusi, V. Della Bianca, M. Donini, K. A. Nadalini, F. Rossi, *J. Immunol.* **157**, 4615 (1996); L. A. H. Allen *et al.*, *Blood* **93**, 3521 (1999).
25. N. A. Buchmeier and F. Heffron, *Infect. Immun.* **59**, 2232 (1991); F. Garcia-del Portillo and B. B. Finlay, *J. Cell Biol.* **129**, 81 (1995); K. Uchiya *et al.* *EMBO J.* **18**, 3924 (1999).
26. F. C. Fang, *J. Clin. Invest.* **99**, 2818 (1997).
27. T. R. Garbe, N. S. Hibler, V. Deretic, *Mol. Med.* **2**, 134 (1996).
28. S. O'Brien, P. S. Jaccett, D. B. Lowrie, P. W. Andrew, *Microb. Pathog.* **10**, 199 (1991).
29. S. K. Hoiseth and B. A. Stocker, *Nature* **291**, 238 (1981); J. L. VanCott *et al.* *Nature Med.* **4**, 1247 (1998).
30. J. A. Cox, A. Y. Jeng, N. A. Sharkey, P. M. Blumberg, A. I. Tauber *J. Clin. Invest.* **76**, 1932 (1985).
31. We thank A. Jones, W. Betz, and S. Fadul for assistance with microscopy, B. Hybertson for the use of a chemiluminometer, F. Heffron for the gift of strain

CL1509, L. A. Allen for helpful discussions, and R. Faust and P. Heyworth for the antibody against p47phox. This work was supported by an NIH postdoctoral fellowship, NIH grants AI39557 and AI44486, the James Biundo Foundation, and grants from Biotechnology and Biological Sciences Research Council, the Wellcome Trust, and the Medical Research Council (UK).

8 November 1999; accepted 18 January 2000

## Resonant Formation of DNA Strand Breaks by Low-Energy (3 to 20 eV) Electrons

Badia Boudaïffa, Pierre Cloutier, Darel Hunting, Michael A. Huels,\* Léon Sanche

Most of the energy deposited in cells by ionizing radiation is channeled into the production of abundant free secondary electrons with ballistic energies between 1 and 20 electron volts. Here it is shown that reactions of such electrons, even at energies well below ionization thresholds, induce substantial yields of single- and double-strand breaks in DNA, which are caused by rapid decays of transient molecular resonances localized on the DNA's basic components. This finding presents a fundamental challenge to the traditional notion that genotoxic damage by secondary electrons can only occur at energies above the onset of ionization, or upon solvation when they become a slowly reacting chemical species.

The genotoxic effects of ionizing radiations ( $\beta$ -,  $x$ -, or  $\gamma$ -rays) in living cells are not produced by the mere direct impact of the primary high-energy quanta. Instead, mutagenic, recombinogenic, and other potentially lethal DNA lesions (1-3), such as single- and double-strand breaks (SSBs and DSBs), are induced by secondary species generated by the primary ionizing radiation (4). Free secondary electrons, with energies between  $\sim 1$  and 20 eV, are the most abundant ( $\sim 5 \times 10^4$  per MeV) of these secondary species (5-8), but it is unclear whether such low-energy electrons are able to induce genotoxic damage, such as SSBs or DSBs (9). To investigate this question, we have irradiated plasmid DNA with a very low energy electron (LEE) source under ultrahigh vacuum (UHV) conditions, because condensed-phase electron-molecule interactions are highly sensitive to minor impurities (10, 11). Our previous work on small bio-organic molecules (12-15) allowed us to develop and adapt the necessary electron microbeam techniques to determine the effects of very low energy, nonthermal secondary electrons on the entire DNA molecule at various well-defined incident elec-

tron energies between 3 and 20 eV. The experiments were performed at  $10^{-9}$  torr in a hydrocarbon-free environment, and all sample manipulation occurred in a sealed glove box under a pure dry nitrogen atmosphere.

Plasmid DNA [pGEM 3Z(-), 3199 base pairs] was extracted from *Escherichia coli* DH5 $\alpha$ , purified, and resuspended in nanopure water (without any tris or EDTA). An aliquot of this pure aqueous DNA solution was deposited onto chemically clean tantalum substrates held at liquid nitrogen temperatures, lyophilized with a hydrocarbon-free sorption pump at 0.005 torr (16), and transferred directly to the UHV chamber without exposure to air or further characterization. After evacuation ( $\sim 24$  hours), the room-temperature DNA solids were irradiated with a monochromatic LEE beam for a specific time at a fixed beam current density ( $2.2 \times 10^{12}$  electrons  $s^{-1} cm^{-2}$ ) and incident electron energy. Thus, the LEE irradiations were performed on clean DNA containing its structural water (17). The DNA was then analyzed by agarose gel electrophoresis and quantified as supercoiled (undamaged), nicked circle (SSB), full-length linear (DSB), and short linear forms; the first three species produce well-resolved bands, whereas the latter produces a smear.

The measured DNA damage yields (Fig. 1) show three striking characteristics. First, very low energy electron irradiation can induce substantial damage in DNA, namely SSBs and DSBs, even at electron energies well below the ionization limit of DNA (7.5

to 10 eV) (18). Second, DNA damage by 3- to 20-eV electrons is highly dependent on the initial kinetic energy of the incident electron, particularly below 14 to 15 eV, where we observed thresholds near 3 to 5 eV and intense peaks near 10 eV. This is in sharp contrast to DNA strand breaks induced by similarly energetic photons, where both SSBs and DSBs have been found to increase monotonically above a threshold near 7 eV and remain relatively constant above  $\sim 12$  eV (19), up to  $\sim 2$  keV (20). Third, the SSB and DSB peak yield values measured here above 7 eV ( $8.2 \times 10^{-4}$  and  $2 \times 10^{-4}$  strand breaks per incident electron, respectively, at the 10-eV peak) are roughly one to two orders of magnitude larger than those for 10- to 25-eV photons (20). For 7- to 25-eV photons, the ratio of SSBs to DSBs is about 30:1, whereas for 7- to 20-eV electrons it is about 4:1 on average. Thus, the mechanisms of DNA damage depend not only on the quantum of energy absorbed, but also on the nature of the particle that deposits the energy.

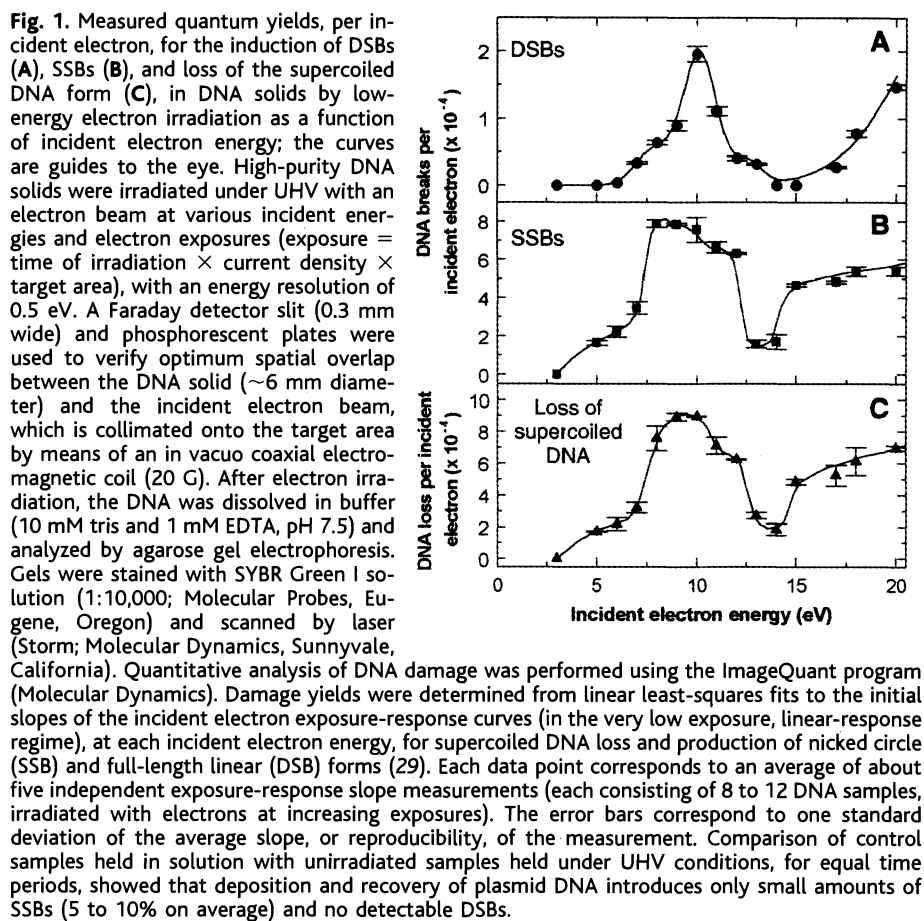
The strong electron energy dependence of the DNA strand breaks, observed here below 14 eV, is attributed to electron attachment somewhere within the DNA molecule, followed by localized bond rupture and subsequent reactions of the fragmentation products. Electron attachment (21) is best illustrated by the type of damage it induces in thin films consisting of very small molecules, such as thymine (13), H<sub>2</sub>O (22), or a deoxyribose analog (14) (Fig. 2). These and other electron impact experiments (15), including some on small linear (23, 24) and cyclic (11, 12, 25) hydrocarbons, have shown that electrons with energies below 15 eV initiate fragmentation of small molecules essentially by attachment of the incident electron; this leads to the formation of a resonance, namely, a transient molecular anion (TMA) state. For a molecule RH this corresponds to  $e^- + RH \rightarrow RH^{*-}$ , where the  $RH^{*-}$  has a repulsive potential along the R-H bond coordinate. This TMA can decay by electron autodetachment (26) or by dissociation along one, or several (12, 14, 25), specific bonds such as  $RH^{*-} \rightarrow R' + H^-$ .

The probability for attachment and subsequent decay via either channel is in part defined by the repulsiveness of the  $RH^{*-}$  potential energy surface and its uncertainty energy width  $\Gamma = \hbar/\tau$ , where  $\hbar$  is Planck's constant divided by  $2\pi$  and  $\tau$  is the electron autodetachment

Canadian Medical Research Council Group in Radiation Sciences, Department of Nuclear Medicine and Radiobiology, Faculty of Medicine, University of Sherbrooke, Québec J1H 5N4, Canada.

\*To whom correspondence should be addressed. E-mail: mhuels01@courrier.usherb.ca

REPORTS



lifetime (typically  $10^{-14}$  to  $10^{-13}$  s) of the TMA as given by the Heisenberg uncertainty principle. In quantum terms, electron attachment is allowed via a vertical electronic transition to the state  $RH^{*-}$  only at energies for which there is sufficient overlap between the nuclear wave functions of the initial ground-state neutral and final anion states. This corresponds conceptually to a reflection of the RH ground-state wave function (of Gaussian shape) by the repulsive curve  $RH^{*-}$ , giving rise to the peaks in the anion fragment yields shown in Fig. 2.

The branching ratio between electron auto-detachment and bond dissociation depends in part on the above intrinsic characteristics of the specific TMA, whereas the final damage yields also depend on extrinsic effects (10) such as electron energy losses or fragment reactions, any of which depend on the structural and chemical composition of the immediate molecular environment. The latter will thus modify the resonant response of the pure individual components of DNA (Fig. 2) when localized within a DNA double strand (Fig. 1). Nonresonant electronic excitations to neutral states  $RH^*$  may also lead to bond cleavage and are allowed at any energy above a threshold, thus contributing a monotonically rising signal to the final anion yields in Fig. 2 above  $\sim 12$  to 13 eV.

On the basis of our measurements, the rel-

ative dimensions of the various DNA components, and the quantum size of the incident electron, we conclude that the observed DNA strand breaks (Fig. 1, below 14 eV) are initiated by resonant electron attachment to the various basic DNA components (base, deoxyribose, phosphate, or hydration  $H_2O$ ), followed by bond dissociations within the TMA's lifetime, usually femtoseconds. Although this event itself may generate a SSB, the observation of DSBs at incident electron energies well below those required for two ionizations ( $>20$  eV) within 10 base pairs of each other on opposing phosphate-sugar strands (19) suggests that some fragmentation products subsequently react locally with other DNA components, leading to a doubly damaged site with breaks on opposing strands. This is supported by the observation of electron-initiated fragment reactions (such as hydrogen abstraction, dissociative charge transfer, atom and functional group exchange, and reactive scattering) occurring over distances comparable to the DNA's double-strand diameter ( $\sim 2$  nm) in condensed films containing water (27) or small linear and cyclic hydrocarbons (11, 24). The 5.5- to 6-eV shoulder observed in the SSB yield curve (but not the DSB yield curve) is possibly related to various electron-induced fragmentation channels observed in gas-phase cytosine and thymine below 10 eV

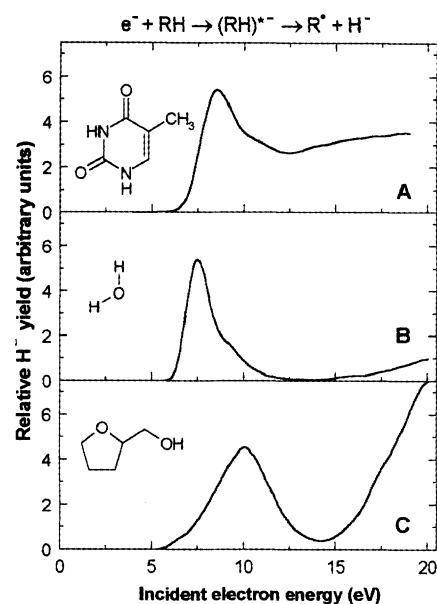


Fig. 2. Electron damage to condensed films of molecules  $RH =$  thymine (A), water (B), and tetrahydrofurfuryl alcohol (C), exemplified in the form of electron energy-dependent desorption yields of energetic  $H^-$  (1 to 4 eV). These and other fragments emanate from the thin films during electron impact as a result of the formation and subsequent dissociation of electron-molecule resonances  $RH^{*-}$ . Each film was  $\sim 5$  monolayers thick and was prepared and irradiated under UHV conditions ( $10^{-10}$  torr). Experimental methods were as described (14, 22).

(12) (or equivalent fragmentations in adenine or guanine).

Our results suggest that the abundant low-energy (1 to 20 eV) secondary electrons, and most likely their ionic and radical reaction products, play a crucial role in the nascent stages of DNA radiolysis and may already induce substantial damage long before their thermalization, or the diffusion limited reactions of other slowly diffusing secondary species produced along ionizing radiation tracks. Because the type of resonant electron-molecule interactions that we observed occur in small molecules regardless of their aggregation state (28), they are expected to be operative in living cells as well. It is only through a complete understanding of such early events in the generation of genotoxic damage that we may hope to eventually manipulate the effects of ionizing radiation at a molecular level.

References and Notes

1. J. F. Ward, in *Advances in Radiation Biology* 5, J. T. Lett and H. Adler, Eds. (Academic Press, New York, 1977), pp. 181-239.
2. O. Yamamoto, in *Aging, Carcinogenesis and Radiation Biology*, K. Smith, Ed. (Plenum, New York, 1976), pp. 165-192.
3. A. F. Fuciarelli and J. D. Zimbrick, Eds., *Radiation Damage in DNA: Structure/Function Relationships at Early Times* (Battelle, Columbus, OH, 1995).
4. C. von Sonntag, *The Chemical Basis for Radiation Biology* (Taylor and Francis, London, 1987).
5. International Commission on Radiation Units and

- Measurements, *ICRU Report 31* (ICRU, Washington, DC, 1979).
6. S. M. Pimblott and J. A. LaVerne, in (3), pp. 3–12.
  7. V. Cobut et al., *Radiat. Phys. Chem.* **51**, 229 (1998).
  8. D. Srdoc et al., in *IAEA CRP Atomic and Molecular Data for Radiotherapy and Radiation Research*, M. Inokuti, Ed. (IAEA Press, Vienna, 1995), chapter 8.
  9. The only previous low-energy work concerned DNA damage by 25- to 4000-eV electrons [see M. Folkard et al., *Int. J. Radiat. Biol.* **64**, 651 (1993)]. In that study, the samples were exposed to high background gas pressures ( $10^{-5}$  to  $10^{-6}$  torr) and contained salt (EDTA, ratio of DNA to EDTA = 1:1 by weight) during electron irradiation; the latter was reported to shield the DNA toward low-energy electrons.
  10. M. A. Huels, L. Parenteau, L. Sanche, *J. Chem. Phys.* **100**, 3940 (1994).
  11. ———, *Chem. Phys. Lett.* **279**, 223 (1997).
  12. M. A. Huels, I. Hahndorf, E. Illenberger, L. Sanche, *J. Chem. Phys.* **108**, 1309 (1998).
  13. L. Sanche, unpublished data.
  14. D. Antic, L. Parenteau, M. Lepage, L. Sanche, *J. Phys. Chem.* **103**, 6611 (1999).
  15. For a review, see A. D. Bass and L. Sanche, *Radiat. Environ. Biophys.* **37**, 243 (1998).
  16. Each sample consisted of 500 ng of purified DNA in 10  $\mu$ l of nanopure water, which was deposited on a tantalum substrate over a measured area of  $\sim$ 6 mm average diameter. After lyophilization, this results in a pure solid calculated to have an average thickness of 10 nm at a known density of 1.7 g  $\text{cm}^{-3}$  assuming minimal clustering of the plasmids in the solid.
  17. Desiccation leaves plasmid DNA with its structural water of about 2.5 water molecules per base pair [S. G. Swartz, M. D. Sevilla, D. Becker, C. J. Tokar, K. T. Wheeler, *Radiat. Res.* **129**, 333 (1992)], with the plasmid solids containing a mixture of A and C conformations. Removal of this intrinsic hydration water is believed to lead to substantial conformational changes and DSBs, which are not observed in our unirradiated control samples held under UHV.
  18. A. O. Colson, B. Besler, M. D. Sevilla, *J. Phys. Chem.* **96**, 9787 (1992).
  19. K. Hieda, *Int. J. Radiat. Biol.* **66**, 561 (1994).
  20. B. D. Michael et al., in (3), pp. 251–258.
  21. For a review, see L. Sanche, *Scanning Microsc.* **9**, 619 (1995).
  22. P. Rowntree, L. Parenteau, L. Sanche, *J. Chem. Phys.* **94**, 8570 (1991).
  23. ———, *J. Phys. Chem.* **95**, 4902 (1991).
  24. A. D. Bass, L. Parenteau, M. A. Huels, L. Sanche, *J. Chem. Phys.* **109**, 8635 (1998).
  25. M. Stepanovic, Y. Pariat, M. Allan, *J. Chem. Phys.* **110**, 11376 (1999).
  26. For vertical electron attachment energies in gas-phase nucleobases below 5 eV, see K. Aflatooni, G. A. Gallup, P. D. Burrow, *J. Phys. Chem. A* **102**, 6205 (1998); for detachment energies in solvated uracil cluster anions, see J. H. Hendricks, S. A. Lyapustina, H. L. de Clercq, K. H. Bowen, *J. Chem. Phys.* **108**, 8 (1998).
  27. M. T. Sieger, W. C. Simpson, T. M. Orlando, *Nature* **394**, 554 (1998).
  28. L. G. Christophorou, E. Illenberger, W. Schmidt, Eds., *Linking the Gaseous and Condensed Phases of Matter: The Behavior of Slow Electrons* (Plenum, New York, 1994).
  29. Sample exposure-response curves can be seen at Science Online ([www.sciencemag.org/feature/data/1044957.shl](http://www.sciencemag.org/feature/data/1044957.shl)).
  30. We thank A. J. Waker for helpful comments and suggestions. Supported by the Medical Research Council of Canada.

30 August 1999; accepted 7 January 2000

## Dual Signaling Regulated by Calcyon, a D1 Dopamine Receptor Interacting Protein

Nelson Lezcano,<sup>1</sup> Ladislav Mrzljak,<sup>2</sup> Steven Eubanks,<sup>1</sup> Robert Levenson,<sup>3</sup> Patricia Goldman-Rakic,<sup>2</sup> Clare Bergson<sup>1\*</sup>

The synergistic response of cells to the stimulation of multiple receptors has been ascribed to receptor cross talk; however, the specific molecules that mediate the resultant signal amplification have not been defined. Here a 24-kilodalton single transmembrane protein, designated calcyon, we functionally characterize that interacts with the D1 dopamine receptor. Calcyon localizes to dendritic spines of D1 receptor-expressing pyramidal cells in prefrontal cortex. These studies delineate a mechanism of  $G_q$ - and  $G_s$ -coupled heterotrimeric GTP-binding protein-coupled receptor cross talk by which D1 receptors can shift effector coupling to stimulate robust intracellular calcium ( $\text{Ca}^{2+}$ ) release as a result of interaction with calcyon. The role of calcyon in potentiating  $\text{Ca}^{2+}$ -dependent signaling should provide insight into the D1 receptor-modulated cognitive functions of prefrontal cortex.

Dopamine (DA), acting through D1 receptors, modulates synaptic transmission in neural circuits, which mediate learning and memory (1, 2). In heterologous expression systems, D1 DA receptors stimulate formation of adenosine 3',5'-monophosphate (cAMP) by coupling to  $G_s$  heterotrimeric GTP-binding (G) proteins (3). However, in brain and kidney, D1 receptor agonists also produce increases in inositol 1,4,5-trisphosphate ( $\text{IP}_3$ ) turnover and intracellular calcium ( $\text{Ca}^{2+}$ ) (4). It is not yet known whether production of these second messengers

involves linkage of D1 receptors to multiple G proteins or activation of alternative D1-like receptor subtypes.

We conducted a yeast two-hybrid screen (5) with the COOH-terminal 81 residues (residues 365 to 446) of the human D1 (hD1) receptor used as bait (6). One interacting clone, designated calcyon (for "calcium on"), contained a cDNA encoding a 217-residue protein (7). Calcyon is a putative type II membrane protein with a predicted single transmembrane segment extending from residues 88 to 103 (8). BLAST searches of GenBank databases indicated that calcyon displays a high degree of sequence similarity with two previously identified proteins of unknown function, P19 and P21 (9). The three proteins exhibit extensive sequence similarity (7). Calcyon appears to be the most highly diverged member of the P19/21/calcyon family of proteins.

Antibodies to a 20-residue segment of calcyon bound to a strong band of about 34 kD and a weaker band of about 28 kD on immunoblots of microsomal protein fractions purified from rhesus monkey brain and spleen (7, 10). The bands were present in samples prepared from prefrontal cortex and caudate putamen but not spleen. Preincubation of antibodies with immunizing peptide prevented detection of the bands. The predicted calcyon protein includes a potential N-linked glycosylation site at residue 73 (7). After digestion of prefrontal cortex microsomal proteins with N-glycosidase F, calcyon antibodies reacted with an  $\sim$ 24-kD protein, suggesting that the 28- and 34-kD bands corresponded to calcyon protein modified by N-linked oligosaccharides (7). Chaotropic salts failed to solubilize the immunoreactive protein, consistent with the notion that calcyon is an integral membrane protein (10). Together, these results suggest an  $\text{NH}_2$ -terminal extracellular, COOH-terminal intracellular transmembrane orientation of calcyon.

Calcyon antibodies labeled cell bodies and processes of neurons throughout the cerebral cortex and hippocampus (11) (Fig. 1, B and F). The labeling was characterized by high density in the vicinity of the plasma membrane and variably in neuronal processes. D1 receptors exhibit a similar distribution in these brain regions (Fig. 1, A and E). Calcyon appears to be preferentially expressed in pyramidal neurons, but expression in interneurons cannot be discounted until a more detailed anatomic investigation is conducted. Extensive labeling was also observed in many other subcortical structures (Fig. 1D). Omission of calcyon antibodies, or preincubation of antibodies with the immunizing peptide, prevented neuronal labeling. Immunogold electron microscopy of prefrontal cortex further revealed calcyon protein in small and medium-sized dendrites and den-

<sup>1</sup>Department of Pharmacology and Toxicology, Medical College of Georgia, Augusta, GA 30912-2300, USA. <sup>2</sup>Section of Neurobiology, Yale School of Medicine, New Haven, CT 06510, USA. <sup>3</sup>Department of Pharmacology, Pennsylvania State College of Medicine, Hershey, PA 17033, USA.

\*To whom correspondence should be addressed. E-mail: cbergson@mail.mcg.edu